Deep-Sea Research II 77-80 (2012) 70–81

Contents lists available at SciVerse ScienceDirect

Deep-Sea Research II

journal homepage: www.elsevier.com/locate/dsr2

# A new estimate of the global 3D geostrophic ocean circulation based on satellite data and in-situ measurements

S. Mulet[a,*], M.-H. Rio[a], A. Mignot[a,1,2], S. Guinehut[a], R. Morrow[b]

[a] CLS-Space Oceanography Division, 8-10 rue Hermès, 31526 Ramonville St. Agne, France
[b] LEGOS-OMP, 18 av. Edouard Belin, 31401 Toulouse Cedex 9, France

ARTICLE INFO

Available online 2 May 2012

*Keywords:*
Geostrophic flow
Thermal wind equation
Meridional oceanic circulation
Observation based product
Remote sensing
Altimetry

ABSTRACT

A new estimate of the Global Ocean 3D geostrophic circulation from the surface down to 1500 m depth (Surcouf3D) has been computed for the 1993–2008 period using an observation-based approach that combines altimetry with temperature and salinity through the thermal wind equation. The validity of this simple approach was tested using a consistent dataset from a model reanalysis. Away from the boundary layers, errors are less than 10% in most places, which indicate that the thermal wind equation is a robust approximation to reconstruct the 3D oceanic circulation in the ocean interior. The Surcouf3D current field was validated in the Atlantic Ocean against in-situ observations. We considered the ANDRO current velocities deduced at 1000 m depth from Argo float displacements as well as velocity measurements at 26.5°N from the RAPID-MOCHA current meter array. The Surcouf3D currents show similar skill to the 3D velocities from the GLORYS Mercator Ocean reanalysis in reproducing the amplitude and variability of the ANDRO currents. In the upper 1000 m, high correlations are also found with in-situ velocities measured by the RAPID-MOCHA current meters. The Surcouf3D current field was then used to compute estimates of the Atlantic Meridional Overturning Circulation (AMOC) through the 25°N section, showing good comparisons with hydrographic sections from 1998 and 2004. Monthly averaged AMOC time series are also consistent with the RAPID-MOCHA array and with the GLORYS Mercator Ocean reanalysis over the April 2004–September 2007 period. Finally a 15 years long time series of monthly estimates of the AMOC was computed. The AMOC strength has a mean value of 16 Sv with an annual (resp. monthly) standard deviation of 2.4 Sv (resp. 7.1 Sv) over the 1993–2008 period. The time series, characterized by a strong variability, shows no significant trend.



## 1. Introduction

The accurate measurement of the ocean 3D circulation is a key issue for a number of scientific challenges, including monitoring the Meridional Overturning Circulation, or calculating ocean heat transports. General circulation models provide 3D current velocities on regional or global scales. They are a precious tool to carry out in-depth studies of the different ocean mechanisms, such as the Meridional Overturning Circulation (Cabanes et al., 2008). For many ocean applications, model reanalysis is needed to provide homogeneous, long-term time series. For instance, the SODA reanalysis (Carton et al., 2000a, 2000b) was used by Zheng and Giese (2009) to study the global ocean heat transport. Reanalysis projects require a huge amount of work in reprocessing data series of the global, high resolution 3D ocean models. Moreover, their validation is strongly dependent on the existence of independent observed currents.

In-situ measurements of the ocean currents at depth are routinely made at only a few specific locations and in the framework of specific national or international programs like RAPID-MOCHA (Cunningham et al., 2007). In synergy with satellite observations, which provide a global, repetitive view of the surface ocean state, the Argo array was launched in 2004 with the objective of providing a global, $3^\circ \times 3^\circ$ array of in-situ estimate of the ocean temperature and salinity from the surface down to 1500–2000 m. In order to take advantage of the numerous, high quality and complementary satellite and in-situ oceanic measurements, observation-based products have been developed (Larnicol et al., 2006; Willis et al., 2003; Willis and Fu, 2008; Willis, 2010) in which different observations are combined using statistics, optimal analysis or simple equations (but no numerical model). These observation-based products are a simpler alternative

* Corresponding author. Tel.: +33 5 61 39 37 36; fax: +33 5 61 39 37 82.
*E-mail addresses:* smulet@cls.fr, sandrine.mulet@cls.fr (S. Mulet), mrio@cls.fr (M.-H. Rio), mignot@obs-vlfr.fr (A. Mignot), sguinehut@cls.fr (S. Guinehut), rosemary.morrow@legos.obs-mip.fr (R. Morrow).
[1] Now at: CNRS, UMR 7093, Laboratoire d'Océanographie de Villefranche, 06230 Villefranche-sur-Mer, France.
[2] Also at: Université Pierre et Marie Curie-Paris 6, UMR 7093, Laboratoire d'Océanographie de Villefranche, 06230 Villefranche-sur-Mer, France.

0967-0645/$ - see front matter © 2012 Elsevier Ltd. All rights reserved.
http://dx.doi.org/10.1016/j.dsr2.2012.04.012

to data assimilation using numerical models and are very useful to validate the accuracy of the model simulations and the impact of its dynamics. Two 3D observation-based products have been developed at CLS. The first product is a so called "synthetic" 3D thermohaline field deduced from a statistical projection of altimetry and Sea Surface Temperature (SST), available from the surface down to 1500 m (Guinehut et al., 2004, 2012). The second one is a new 3D oceanic geostrophic circulation field described in the present paper.

Flow in the ocean interior (away from the boundary layers) and away from the equator is in geostrophic balance to the first order as suggested by observations and scaling arguments (Wunsch, 1996, chapter 2), even in boundary currents such as the Atlantic Deep Western Boundary Current (Johns et al., 2005). In this paper, the 3D oceanic circulation is computed assuming geostrophic balance and using the thermal wind equation, taking the reference level at the surface where the geostrophic currents are well known and derived from altimetric sea level heights. The horizontal density gradient in the thermal wind equation is provided by the synthetic thermohaline field mentioned above. Global weekly, monthly and yearly 3D oceanic currents from the surface down to 1500 m (hereafter called the Surcouf3D Currents) have been calculated from 1993 to 2008.

In the first part of this paper, we check the validity of the approach by applying the thermal wind equation to a consistent oceanic data set from the GLORYS1V1 model reanalysis (Ferry et al., 2010; Lique et al., 2011). We then compare the Surcouf3D currents to in-situ data in the Atlantic Ocean where there is a strong oceanic overturning circulation. It is also the most observed ocean which makes the validation easier. We validate the weekly reanalysis at 1000 m depth through a comparison with in-situ velocities from Argo floats (Ollitrault et al., 2006; Ollitrault and Rannou, 2010) and modeled velocities from the GLORYS1V1 reanalysis. Comparisons are also made with the RAPID-MOCHA current meters located in the western boundary current at 26.5°N. In the last part of the paper, we use the Surcouf3D currents to estimate the Meridional Overturning Circulation (MOC). Two time series are computed. The first one, at 25°N, spans the 1993–2008 period and is compared to previous results by Bryden et al. (2005) (referred as BR05 subsequently), calculated from full-depth hydrographic sections. The second time series, computed at 26.5°N, spans the 2004–2007 period and is compared with results from GLORYS1V1 reanalysis and the RAPID-MOCHA monitoring project. In both cases, monthly means of the Surcouf3D currents are used in order to focus on the seasonal and interannual variability of the MOC.

The paper is organized as follows. After presenting the data in Section 2 and describing the computation method of the Surcouf3D currents in Section 3, Section 4 is dedicated to the comparisons with other existing products. The 1993–2008 and 2004–2007 time series of the monthly estimated AMOC through the 25°N and 26.5°N sections are analyzed in Section 5. Discussion and conclusions are given in Section 6.

## 2. Data

Five types of data are used in this study. The first two types (altimetric measurements and the synthetic thermohaline field) are used in the computation of the 3D geostrophic velocities while the three other ones (GLORYS reanalysis, estimates of Argo float velocities and current meter measurements from the RAPID-MOCHA database) are used for validation purposes.

### 2.1. Gridded maps of surface altimetric geostrophic currents

We use weekly 1/3° resolution maps of delayed-time geostrophic surface currents computed by the SSALTO/DUACS center and distributed by AVISO from January 1993 to December 2008 (SSALTO/DUACS, 2011). The altimetric data used in the computation of the multimission maps of Sea Level Anomaly (SLA) are from the ERS-1,2, ENVISAT, Topex/Poseidon, Jason-1,2, GFO, GEOSAT satellites. The CMDT RIO05 (Rio and Schaeffer, 2005) Mean Dynamic Topography (MDT) is added to the SLA maps to obtain maps of absolute dynamic topography, that are then used to infer the ocean surface currents through geostrophy. When computing absolute geostrophic currents from altimetry, the dominant error comes from the mean circulation. The determination of this error is quite challenging. In Rio and Schaeffer (2005) the MDT is validated using a dataset of independent drifting buoy measurements of the surface current velocities from which the Ekman component is extracted. Altimetric geostrophic velocity anomalies are collocated to the in-situ data and the mean geostrophic currents derived from the RIO05 MDT are used to obtain absolute collocated geostrophic velocities. In the Atlantic Ocean, the Root Mean Square difference between both geostrophic velocity datasets (in-situ and altimetric) is in the order of 12 cm/s for both components of the velocity. This value reduces to less than 9 cm/s away from strong Western Boundary Currents (Rio and Schaeffer, 2005). This RMS value is the sum of different error components (error on the Ekman model, error on the altimetric velocity anomalies, error on the in-situ drifting buoy measurements and error on the RIO05 MDT currents) so that it is an overestimate of the true RIO05 MDT error.

### 2.2. 3D synthetic thermohaline field

The weekly 3D synthetic thermohaline field is an observation-based product deduced from SLA and Sea Surface Temperature (SST) through a statistical projection as described by Guinehut et al. (2004, 2012). The altimeter data come from the SSALTO/DUACS center and are described in Section 2.1. The sea surface temperature fields are Reynolds 1/4° products (Reynolds et al., 2007).

The main idea of the method is to start from a smooth first guess, the monthly ARIVO climatology based on Argo measurement (Gaillard and Charraudeau, 2008) and use high resolution satellite observations to improve it. First the baroclinic component ($H$) of the SLA due to the density variations from the surface to a chosen reference level is extracted using regression coefficients deduced from an altimeter/in-situ comparison study. The regression coefficients have been calculated using collocated dynamic height anomalies computed from Argo temperature and salinity profiles and altimeter SLA (Dhomps et al., 2011; Guinehut et al., 2006). Using a reference level at 1500 m depth or at the bottom in coastal areas shallower than 1500 m, the regression coefficients range from 0.8 in the equatorial and tropical regions to 0.7 and 0.2 in mid to high latitudes with a clear latitudinal dependency. These values mean that most of the altimeter SLA signal is projected onto the vertical ocean structure at low latitudes but that only 70–20% are projected at mid to high latitudes, where the barotropic and deep baroclinic signals are more important.

Secondly, a multiple linear regression method is used (Eq. (1)) to provide temperature ($T'$) and salinity ($S'$) anomalies relative to the monthly ARIVO climatology (Gaillard and Charraudeau, 2008):

$$\begin{aligned} T'(x,y,z,t) &= \alpha(x,y,z,t)H'(x,y,t)+\beta(x,y,z,t)SST'(x,y,t) \\ S'(x,y,z,t) &= \gamma(x,y,z,t)H'(x,y,t) \end{aligned} \tag{1}$$

Here $H'$ and SST$'$ are anomalies of the baroclinic height and sea surface temperature, respectively, relative to the monthly ARIVO climatology. The regression coefficients $\alpha$, $\beta$ and $\gamma$ have spatial and seasonal dependency and are computed from historical in-situ $T/S$ profiles (Argo floats, XBT, CTD) distributed by the ENACT and

Coriolis data centers from 1950 to 2008. They are calculated on a $1^\circ \times 1^\circ$ regular grid using the historical data available in $5^\circ$ latitude $\times$ $10^\circ$ longitude radius of influence around each grid point.

Finally, the ARIVO climatology is added back to the anomalies to compute the synthetic thermohaline field. The heaviest computational step is the evaluation of the regression coefficients. But once they are computed for each map of SLA and SST, it is easy to compute thermohaline fields. These 3D fields are computed weekly on a global $1/3^\circ$ Mercator grid and on 24 Levitus levels from 0 to 1500 m. The first levels to 30 m are spaced by 10 m, and then the space increases to reach 100 m between 300 and 1500 m. The 1500 m reference level was chosen in order to have enough in-situ data to compute statistically significant regression coefficients. Indeed, although many Argo floats descend to 2000 m depth, a majority of the historical floats descend only to 1500 m depth. In addition to the real-time production, reanalyses that use better reprocessed observations (SLA, SST) are regularly generated. For this study, we use a reanalysis of the synthetic thermohaline field that has been computed recently and covers the 1993–2008 period.

The quality of the synthetic fields depends mainly on the relationship that exists between the surface and subsurface fields. For example, the temperature field within the mixed layer is very well constrained by the SST field everywhere. Below the mixed layer, mid to high latitudes are well constrained by the SLA with correlation greater than 0.7 between SLA and temperature at depth. In the tropics, even though the correlation between SLA and temperature at depth is smaller and in the order of 0.4, the projection of mesoscale surface signal still allows us to add information to the first guess (Guinehut et al., 2012). In the regression applied to salinity, only the SLA is used since global and high resolution fields of Sea Surface Salinity observations are not yet available. Improvements are indeed expected with the ongoing SMOS (Silvestrin et al., 2001) and Aquarius missions (Le Vine et al., 2007). Although the correlation between surface SLA and salinity at depth is lower than that between SLA and temperature everywhere, the first guess is again improved by projecting the SLA at depth (Guinehut et al., 2012).

### 2.3. GLobal Ocean ReanalYses and Simulations (GLORYS) field

GLORYS is an ocean general circulation model reanalysis product based on a slightly modified version of the PSY3V2 operational system from Mercator Ocean (Ferry et al., 2010; Lique et al., 2011). The configuration is global on a $1/4^\circ$ ORCA grid with 50 vertical levels. It assimilates SST maps, along track SLA and in-situ *T*/*S* profiles, using the SEEK extended Kalman filtering assimilation technique. The mean dynamic topography (MDT) used to assimilate the SLA is the CMDT RIO05 product (Rio and Schaeffer, 2005) combined with a nearshore numerical model.

Here we use the weekly and monthly averaged 3D velocity fields from the first version of GLORYS (GLORYS1V1), available over the time period 2002–2008.

### 2.4. Argo New Displacement Rannou Ollitrault (ANDRO) observed velocity database

The nominal cycle of an Argo float is to dive down to its parking depth where it drifts for about 10 days, before diving to 2000 m and going back to the surface measuring *T*/*S* profiles. Once at the surface the Argo float is located by satellite several times during a ~12-hour period, where it drifts with the surface currents. The Argo displacement at depth can thus be estimated from the locations of the last float position observed by the satellite at the sea surface before the float dives and of the first one after the float comes back at the surface.

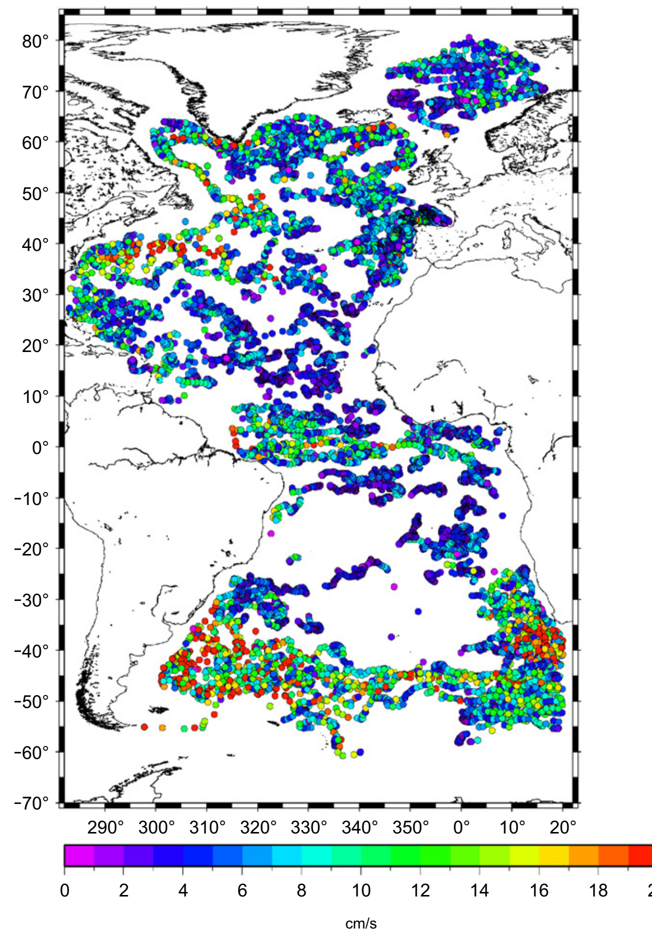


**Fig. 1.** Mean positions and intensities of the mean velocities (cm/s) of the Argo floats from the ANDRO database over their 10-days-displacement at 1000 m depth for the 2006–2007 period.

The ANDRO database (Ollitrault et al., 2006; Ollitrault and Rannou, 2010) contains velocity displacements of the Argo floats at their parking depths (1000 m mostly but also 1500 m and 2000 m) from 2002 to 2007. ANDRO is only based on data distributed by the AOML and Coriolis Data Assembly Centers. The Argo float displacement data have been corrected before computing the drifting velocity. The main corrections concern the parking pressure and the surface positions determined by satellite localization. The error associated with this database is of order 1 cm/s (Ollitrault et al., 2006; Ollitrault and Rannou, 2010).

In this paper we use the ANDRO velocity displacements at 1000 m in the Atlantic Ocean for 2006 and 2007 that represent more than half of the entire ANDRO set (i.e. more than 13,000 velocity estimates). Trajectories of the floats and their velocities are shown in Fig. 1. The ANDRO database, by construction, represents mean velocities over 10 days which are averaged over the drift distance that occurred during these 10 days. The mean displacement ranges from less than 50 km in the center of the sub-tropical gyres to 100–150 km in strong currents such as the Gulf Stream or the Antarctic Circumpolar Current (Fig. 2).

### 2.5. RAPID-MOCHA array

RAPID-MOCHA is a joint program involving the U.K. Rapid Climate Change (RAPID) program and the U.S. Meridional Overturning Circulation and Heatflux Array (MOCHA) project. It consists of around twenty moorings equipped with CTDs and pressure sensors deployed at 26.5°N at the western boundary,

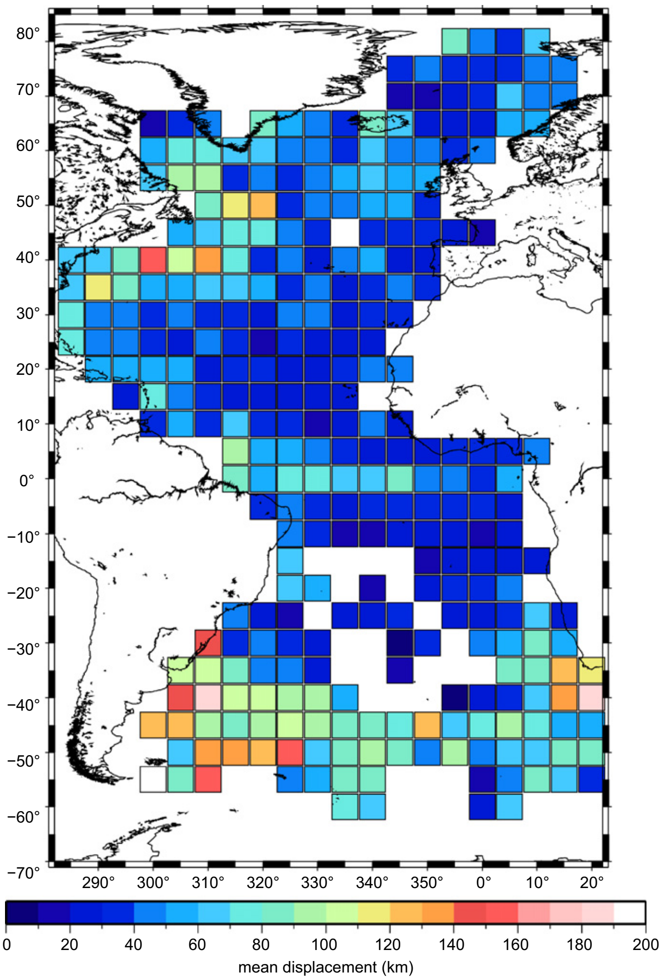


**Fig. 2.** Mean displacement (km) over 10 days of the Argo floats from the ANDRO database at 1000 m depth from January 2006 to December 2007.

around the mid-Atlantic ridge and at the eastern boundary. Current meters have also been deployed at the western boundary to resolve the western boundary currents (Johns et al., 2008). In this study, we used the monthly averaged velocities from the current meters and *T*/*S* profiles at the western boundary deployed in March 2004 and recovered in May 2005.

We also use the monthly averaged Meridional Overturning Circulation (MOC) estimated from April 2004 to September 2007 in the framework of the RAPID-MOCHA project as described by (Cunningham et al., 2007; Kanzow et al., 2007).

## 3. Method

The geostrophic components of the ocean circulation can be computed at all depths $z_i$ using the thermal wind equation:

$$u(z=z_i)=u(z=0)-\frac{g}{\rho f}\int_{z=z_i}^{z=0}\frac{\partial}{\partial y}\rho(z)\,dz$$
$$v(z=z_i)=v(z=0)+\frac{g}{\rho f}\int_{z=z_i}^{z=0}\frac{\partial}{\partial x}\rho(z)\,dz \qquad (2)$$

The first terms on the right hand side of Eq. (2) are the velocity components due to the sea surface slope current while the second terms are the components of baroclinic velocity resulting from horizontal density gradients from the surface to $z=z_i$.

The geostrophic ocean currents at the surface $u(z=0)$, $v(z=0)$ are estimated from the altimetric maps of absolute dynamic topography (computed as the sum of the SLA and the MDT). The densities at depth $\rho(z)$ are computed from the synthetic thermohaline field. We thus obtain weekly 3D grids of current velocities at the same horizontal and vertical resolution as the synthetic thermohaline field (global 1/3° Mercator grid on 24 Levitus levels from the surface to 1500 m). Since the geostrophic approximation is not verified near the equator, no current is estimated in the equatorial band between 5°S and 5°N. Also, there is no estimation where the CMDT RIO05 (Rio and Schaeffer, 2005) or the SLA is not defined, in semi-enclosed seas (Mediterranean, Black and Red seas) and high latitudes. In the following, we will refer to this 3D velocity estimate as Surcouf3D.

Classically, relative velocities are computed from T/S fields using the thermal wind equations assuming a level of no motion. Fig. 3(A) shows the 2006 annual mean velocities obtained from the synthetic thermohaline field and the thermal wind equation assuming a level of no motion at 1500 m. The Surcouf3D currents are displayed in Fig. 3(B). While the relative velocities to 1500 m only resolve, by construction, the baroclinic component of the circulation relative to 1500 m, the Surcouf3D velocities contain both the shallower and deeper baroclinic components and also the barotropic component of the ocean circulation. As a result, the relative velocities to 1500 m are weak compared to the Surcouf3D estimate; the Gulf Stream signature (at 39°N) shows a maximum velocity of around 35 cm/s and a maximum extension of 900 m (Fig. 3A). The Gulf Stream velocity computed with Surcouf3D extends deeper and is clearly stronger (maximum velocities greater than 50 cm/s), in better agreement with the GLORYS current estimate (Fig. 3C). The recirculation cells associated with the Gulf Stream in the Surcouf3D field are also in much better agreement with GLORYS than the relative velocities to 1500 m. Indeed, the westward current at 27°N is better resolved and the long-lived recirculation pattern centered around 35.5°N is modified with an intensification of the westward branch and a slowing down of the eastward branch. Also, north of the Gulf Stream, the Surcouf3D and the GLORYS currents are consistent, with an eastward current at 42°N and a westward current which is deeper and shifted to the south. However, the Surcouf3D velocities are stronger than the GLORYS ones and contain more mesoscale variability at depth. This is more clearly visible in Fig. 4 where the 2006 annual mean horizontal currents at 500 m depth from Surcouf3D and GLORYS are compared in the Gulf Stream region. Both of the Surcouf3D and GLORYS fields are based on the use of altimetry, SST and *T*/*S* profiles, except GLORYS uses a full data assimilation scheme. Despite some small discrepancies, the two fields are in good agreement, which is a very promising result for such a simple velocity computation method as Surcouf3D.

In order to further assess the accuracy of the Surcouf3D and the GLORYS velocity field we will compare them in the next section to independent data (the ANDRO dataset in Sections 4.2 and the RAPID-MOCHA current meter array in Section 4.3).

## 4. Assessment of the Surcouf3D accuracy

### *4.1. Validity of the thermal wind equation*

The assumption made to compute the Surcouf3D field is based on the validity of the thermal wind relation to derive absolute horizontal velocities. In this section, we test this assumption through the use of an ocean model reanalysis GLORYS1V1 over the 2006–2007 periods.

The temperature (*T*), salinity (*S*), height above geoid (*H*) and current (Unat/Vnat) fields from the GLORYS daily reanalysis are first weekly averaged. Then the thermal wind equation is applied using the GLORYS *T*/*S*/*H* fields. The reference level is set at the surface (Eq. (2)), where the velocities are computed from the

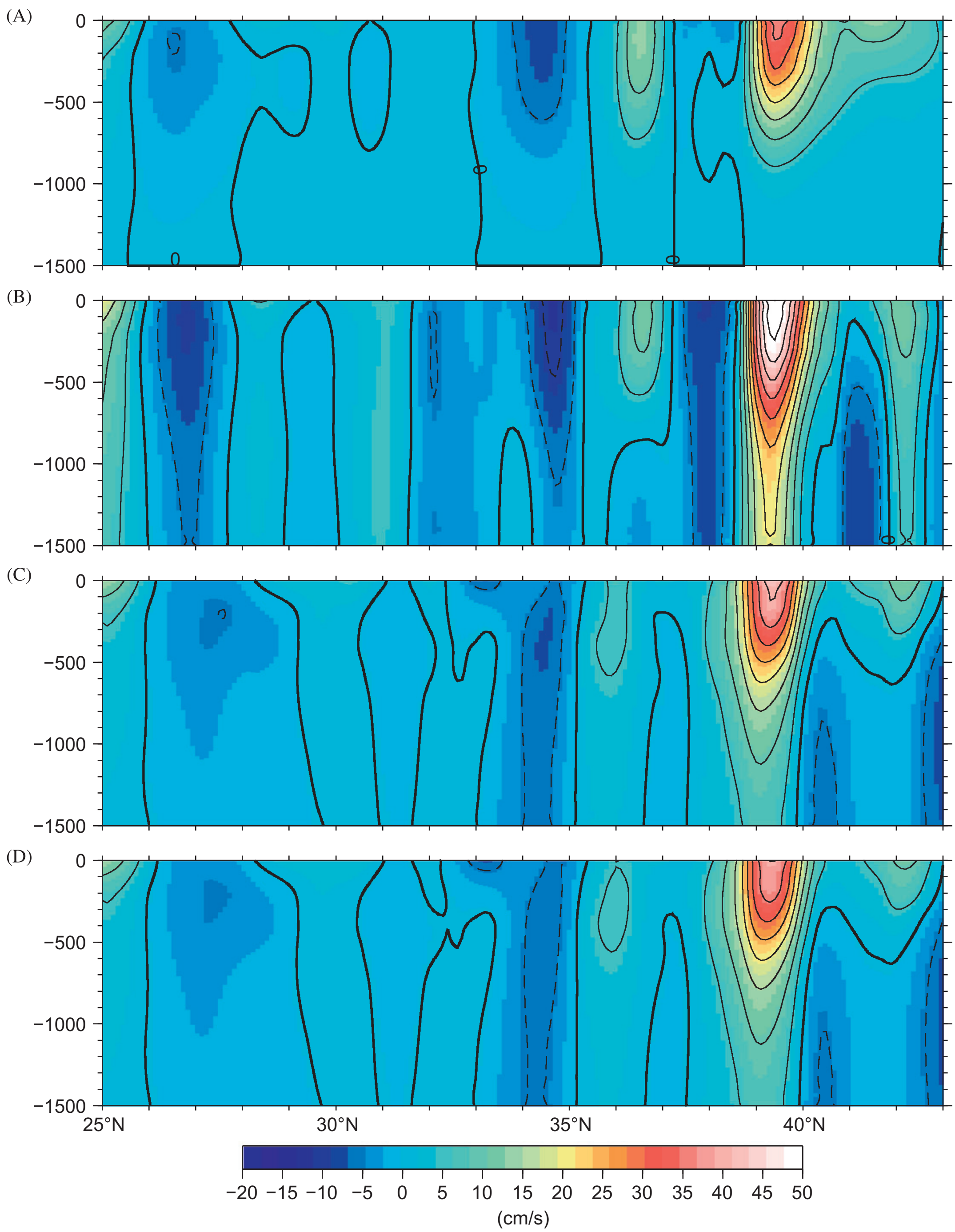


**Fig. 3.** Vertical structures of the 2006 annual mean zonal velocities (cm/s) along a section in the Gulf Stream at 60°W (see black line in Fig. 4) for (A) the velocities relative to 1500 m, (B) Surcouf3D, (C) GLORYS and (D) the geostrophic velocities computed from the *H*/*T*/*S* GLORYS fields through the thermal wind equation.

GLORYS *H* field using the geostrophic approximation. At each vertical level, the geostrophic current field (Ugeo/Vgeo) is reconstructed by integrating the horizontal density gradients computed from the *T*/*S* fields, following Eq. (2). Finally we compared the reconstructed geostrophic current field (Ugeo/Vgeo) with the native current field from GLORYS (Unat/Vnat).

Fig. 3(D) shows the 2006 yearly averaged geostrophic meridional velocities at 60°W reconstructed from GLORYS *H*/*T*/*S* fields. There are very few differences even in the surface layers compared to Fig. 3(C) that shows the same profile for the native GLORYS current field. Thus, the ageostrophic components in GLORYS, including the surface Ekman currents, have very little impact on the annual mean in the Gulf Stream area. In the case of weekly fields, larger differences are obtained near the surface, which are typical of the Ekman circulation (not shown).

Outside the Ekman layer, there is no bias between the reconstructed and the native weekly fields. At 600 m the absolute mean differences are less than 0.1 cm/s both for the zonal and the meridional components. Figs. 5 and 6 show the standard deviation of the differences between the native and the reconstructed currents, computed in $20^\circ \times 20^\circ$ boxes at different depths (Fig. 6) and by latitudinal bands of 20° (Fig. 5). Values are expressed as a percentage of the standard deviation of the native field. In the first 50 m (Figs. 5 and 6A and B) the error is between 20% and 50%. This high surface layer error is due to the Ekman currents which are included in the native currents but not in the reconstructed, geostrophic field.

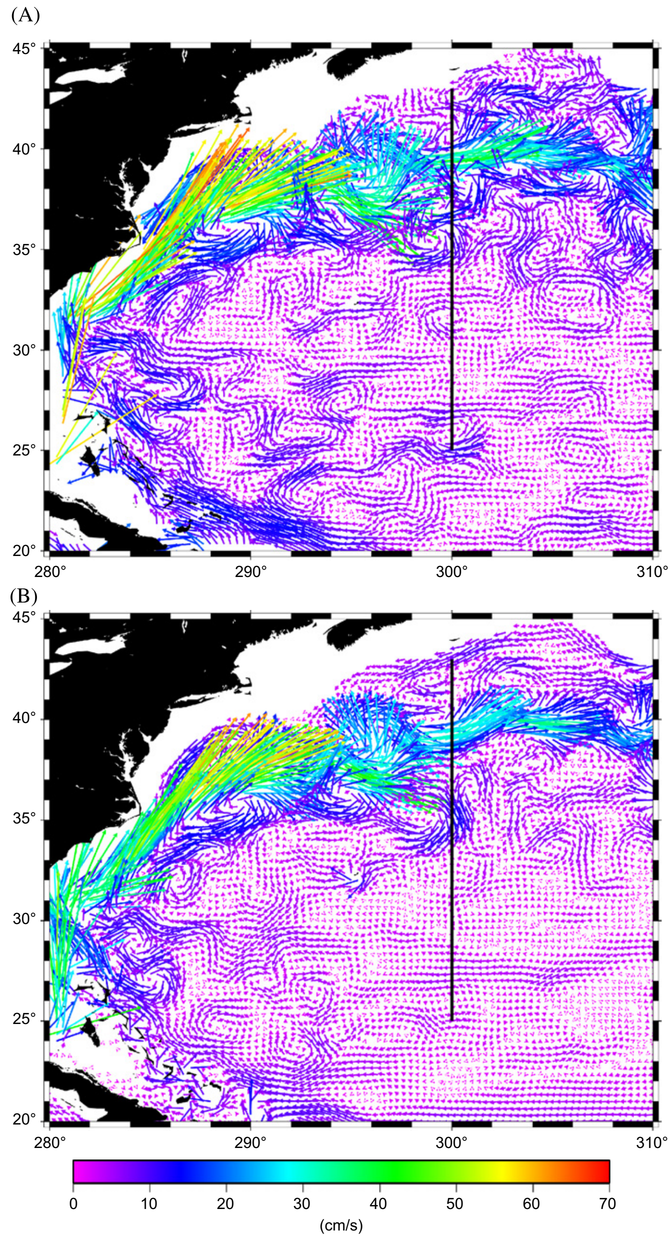


**Fig. 4.** Circulation in 2006 at 500 m depth in the Gulf Stream area from (A) Surcouf3D estimate and (B) GLORYS reanalysis. The black line shows the section at 60°W used in Fig. 3.

Below the Ekman layer, the error is much smaller, less than 12% at depths larger than 500 m (Fig. 5). At 200 m (Fig. 6C and D), in the ocean interior, the error is lower than 10% everywhere, except in the North Atlantic gyre where the error is about 13%. Higher errors also occur closer to the coasts, probably due to other ageostrophic processes. This is the case for the very coastal Western Boundary Currents (East Australian Current, Florida Current), for certain upwelling currents system (Benguela Current, Canary Current) or in complex bathymetric areas (China sea, Gulf of Mexico). However the errors remain less than 20%.

To conclude, we find that with a weekly temporal resolution and a 1/3° grid, the thermal wind equation is a robust approximation to reconstruct the 3D ocean velocity field in the ocean interior with errors lower than 10% in most places. Close to the coasts, where friction becomes non negligible, the error is higher, up to 20%. Errors up to 50% are found near the surface, where the ageostrophic Ekman currents are a significant contribution to the total current.

### 4.2. Comparison to the ANDRO velocity database

We interpolated the observation-based currents (both the Surcouf3D currents and the velocity field relative to 1500 m) and the modeled currents (GLORYS) onto the date and position of the Argo floats drifting at 1000 m in the Atlantic between 2006 and 2007 (see Fig. 1). Then, for each field, a statistical comparison was made with the in-situ Argo float velocities. Results are very similar for the zonal and meridional components (Table 1). In the following, we will only discuss the meridional component, which is weaker and more difficult to estimate accurately.

There is no bias between the Surcouf3D (resp. GLORYS) and ANDRO meridional velocities with a mean difference of 0.35 cm/s (resp. 0.5 cm/s). The amplitudes of the variability of the Surcouf3D and GLORYS meridional components are also very close (standard deviations are respectively 6.92 and 6.95 cm/s) but both are higher than the in-situ observations (5.70 cm/s). This is mainly due to the Argo sampling frequency. The mean displacement of the Argo float in 10 days (Fig. 2) is around 50 km in the whole Atlantic and more than 100 km in region of high variability (south of the southern subtropical gyre, Gulf Stream area) while the resolution of Surcouf3D and GLORYS is 1/3° and 1/4° respectively. Note that while the temporal averaging is consistent between the different data sets, the Argo float velocity is a 10 days lagrangian average estimate whereas the Surcouf3D and GLORYS are representative of eulerian weekly mean fields. Meijers et al. (2011) have quantified the error between this type of lagrangian and eulerian fields to be around 3.9 cm/s near Kerguelen Island.

Both Surcouf3D and GLORYS show a correlation higher than the 99% significance level defined by Emery and Thomson (1998). Surcouf3D shows a good correlation with the Argo drift velocities (0.6) while GLORYS is less consistent (0.42). The standard deviation of the differences to Argo floats is smaller with Surcouf3D (5.75 cm/s) than with GLORYS (6.91 cm/s). The smallest difference is obtained with the velocities calculated relative to 1500 m (5.13 cm/s). However, this relative velocity field fails to resolve the variability of the ocean circulation (the standard deviation is 1.23 cm/s, to be compared with 5.7 cm/s for the Argo floats). In order to have a synthetic vision of these different statistics, we use the skill score ($S_{Taylor}$) defined by Taylor (2001) and given by the following equation:

$$S_{Taylor} = 2\frac{(1+R)}{((\sigma_r/\sigma_f)+(\sigma_f/\sigma_r))^2} \quad (3)$$

where $R$ is the correlation coefficient between the two fields $f$ and $r$ that are compared, $\sigma_f$ and $\sigma_r$ are their standard deviations. The score varies from zero to one. The score approaches one if the two fields that are compared are correlated and have similar variability. The highest skill is obtained with Surcouf3D (0.77) followed by GLORYS (0.68). The relative velocity field is highly penalized (0.14) because it contains very low signal at 1000 m, with much weaker horizontal density gradients here (see also Fig. 3).

### 4.3. Comparison to the RAPID current meter velocities

Velocities at various depths has been routinely measured from April 2004 in the western boundary current off the Bahamas (26.5°N, 76.5°W) by current meters from the RAPID-MOCHA project (Johns et al., 2008). In this study we consider the times series from April 2004 to October 2006. The Surcouf3D monthly velocities, interpolated onto the current meter locations (Fig. 7), show a very good consistency with the current meter velocities over the first 400 m, with a correlation coefficient up to 0.96 at the 99% significance level. For the GLORYS dataset, the correlation coefficient is 0.82. The correlation coefficient decreases with

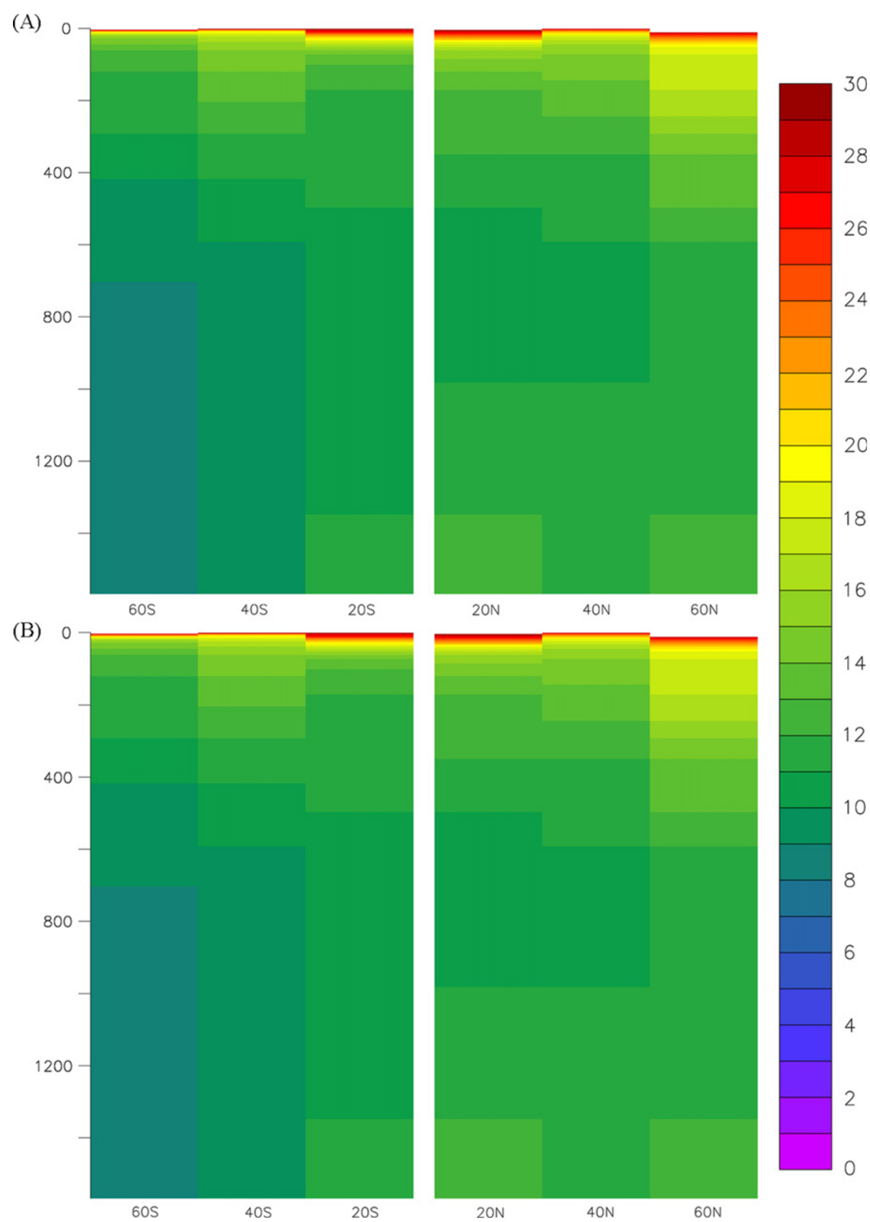


**Fig. 5.** Standard deviation (%) of the differences between the GLORYS native and the reconstructed currents computed by latitudinal bands of 20° and at different depths for (A) the zonal component and (B) the meridional component. Values are expressed as a percentage of the standard deviation of the native field.

depth but the Surcouf3D and RAPID-MOCHA zonal velocities remain correlated. At 800 m, the correlation coefficient is 0.68 at the 99% confidence level and at 1200, where the zonal flow is weak, it is 0.41 at the 95% confidence level.

The RAPID-MOCHA meridional current is directed northward at depths shallower than 800 m, and southward at 1200 m, except for November 2004 when a maximum of northward meridional velocity extends from 100 m to 1200 m and for January 2006. The vertical shear of the meridional current is resolved by the GLORYS currents, but not by the Surcouf3D field. This may be due to the predominance of ageostrophic dynamics, not taken into account by our simple, geostrophic methodology. However, Fig. 6 shows that ageostrophic processes in this area contribute only to 13% of the signal at depth. This is in good agreement with Johns et al. (2005) mentioning that this current is mainly in geostrophical balance. To further check the validity of applying the thermal wind equation to resolve this strong current shear, we have applied our methodology using two *T*/*S* profiles from the RAPID-MOCHA array (at 76.50°W and 76.75°W) and using as reference velocities values the current meter located at 100 m depth at 76.5°W. The obtained currents (dotted red lines in Fig. 7) correctly resolve the inversion of the meridional component around 800 m (Johns et al., 2008). The failure of the Surcouf3D field to resolve the meridional current shear is therefore not due to the geostrophic approximation, but rather to the failure of the synthetic thermohaline field to capture the strong density shear associated with this narrow current system. In the future, we plan to improve the thermohaline field by combining it with Argo float profiles in order to improve locally the description of the ocean 3D *T*/*S* characteristics. Note that the geostrophic meridional velocity profile computed from the RAPID-MOCHA *T*/*S* profiles does not match exactly the current meter measurements (dotted and solid red lines in Fig. 7). This is mainly because these fields do not represent the current at the same location. The current meters give measurements at 76.5°W while the geostrophic meriodional velocity profile is evaluated between the location of the two *T*/*S* profiles (76.5°W and 76.75°W).

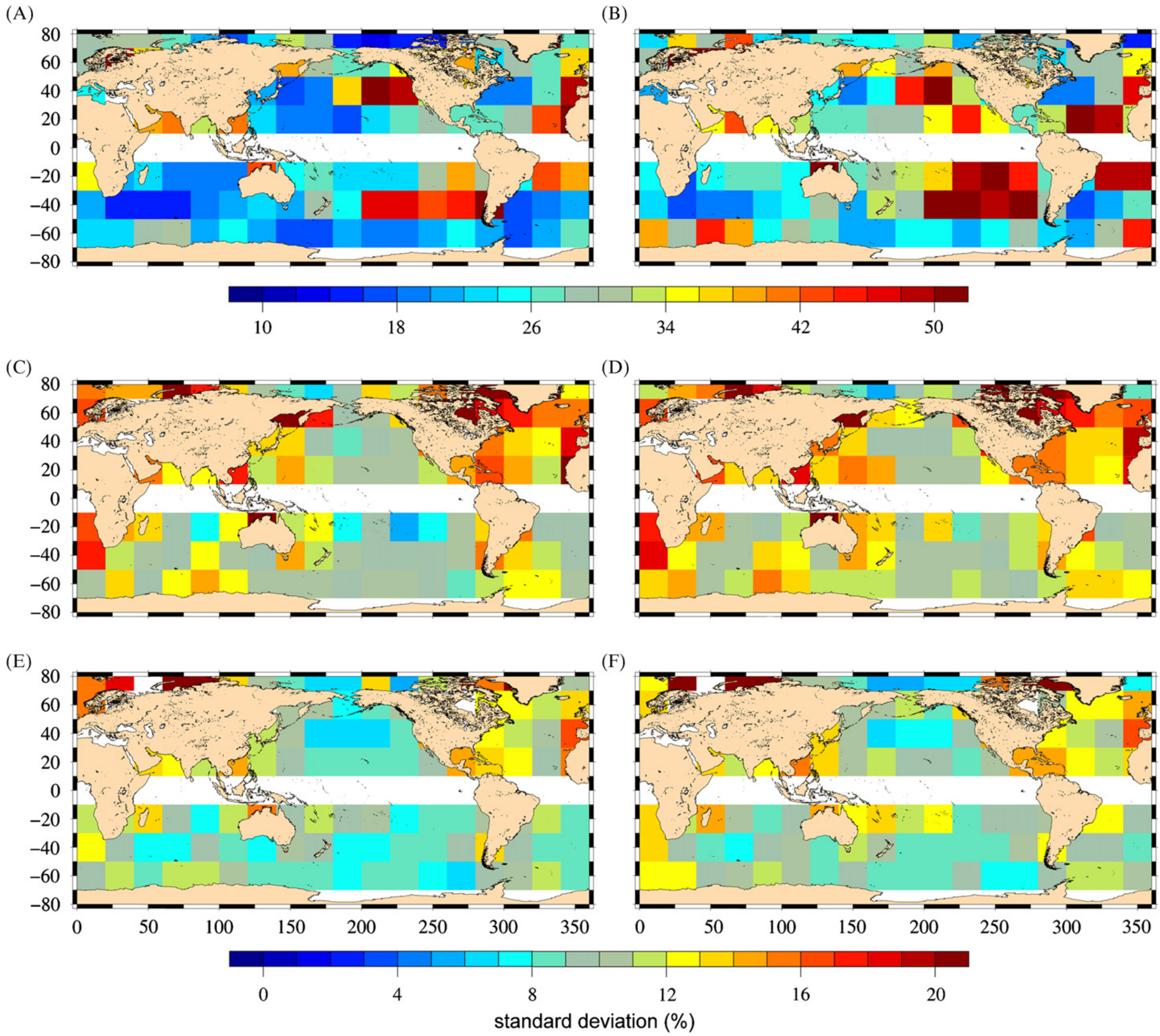


**Fig. 6.** Standard deviation (%) of the differences between the GLORYS native and the reconstructed currents computed in 20° × 20° boxes (A, B) at 10 m, (C, D) at 200 m and (E, F) at 600 m for (left) the zonal component and (right) the meridional component. Values are expressed in percentage of the standard deviation of the native field.

**Table 1**
Results of statistical comparisons of three current fields (Surcouf3D, GLORYS and velocities relative to 1500 m) to Argo floats drifting at 1000 m in the Atlantic over 2006/2007 period.

| | Surcouf3D | | GLORYS | | Velocities relative to 1500 m | | Argo floats (ANDRO database) | |
|---|---|---|---|---|---|---|---|---|
| Velocity components (*U*: zonal, *V*: meridional) | *U* | *V* | *U* | *V* | *U* | *V* | *U* | *V* |
| Standard deviation (cm/s) | 7.27 | 6.92 | 7.23 | 6.95 | 1.31 | 1.23 | 5.97 | 5.70 |
| Correlation coefficient | 0.61 | 0.60 | 0.46 | 0.42 | 0.58 | 0.55 | | |
| Standard deviation of the differences (cm/s) | 5.93 | 5.75 | 6.93 | 6.91 | 5.32 | 5.13 | | |
| Mean difference (cm/s) | −0.22 | 0.35 | 0.10 | 0.50 | −0.18 | 0.13 | | |
| Taylor's score | 0.78 | 0.77 | 0.71 | 0.68 | 0.14 | 0.14 | | |

## 5. Application: monitoring the Atlantic Meridional Oceanic Circulation (AMOC)

According to Kanzow et al. (2007), overturning at 25°N in the Atlantic can be divided into three components: the Florida western boundary transport, the surface Ekman transport and the interior geostrophic transports, the last two being integrated from the Bahamas to Africa. In the traditional approach, only the baroclinic part of the geostrophic transport relative to a reference level is computed, which is why a time variant offset must be added to impose mass conservation. Kanzow et al. (2006) uses bottom pressure sensors to overcome this issue. These sensors

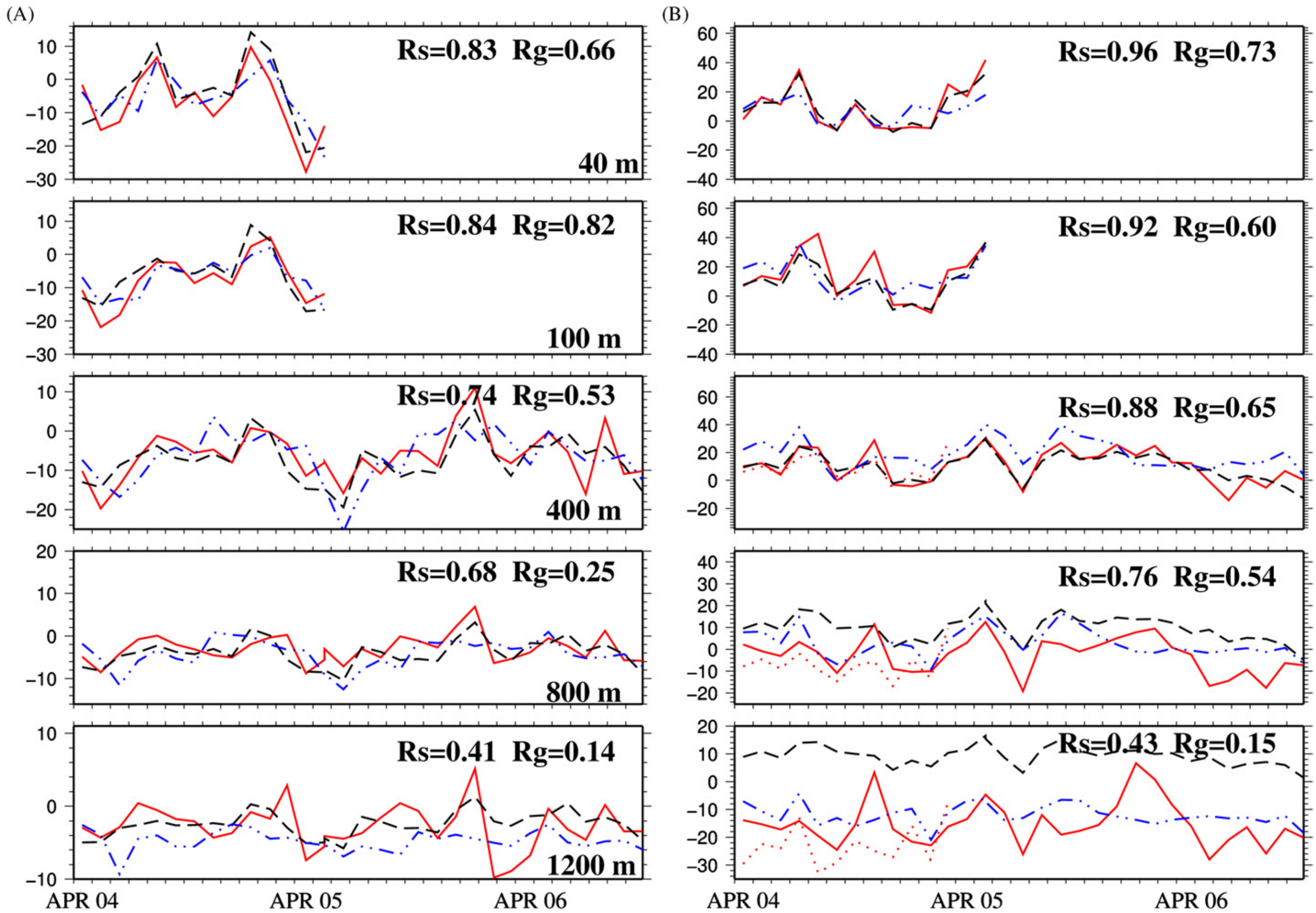


**Fig. 7.** April 2004–2005 time series of the monthly mean (A) zonal and (B) meridional velocities interpolated at the localization of the current meters from RAPID-MOCHA in the western boundary current off the Bahamas. In black dashes: Surcouf3D, in blue dashes and dots: GLORYS, in solid red lines: current meters from RAPID-MOCHA at 76.5°W, and red dots: current computed through the thermal wind equation using *T*/*S* profiles and current meter at 100 m from RAPID-MOCHA. The correlation coefficients with RAPID-MOCHA measurements are written in the top right of each panel, *Rs* refer to correlation with Surcouf3D time series and *Rg* to the GLORYS time series. (For interpretation of the references to color in this figure legend, the reader is referred to the web version of this article.)

cannot measure the absolute pressure with sufficient accuracy but do give access to the bottom pressure fluctuations and thus to the transport relative to the time mean value (Kanzow et al. 2006). While the transport variability can be studied without making any further assumptions, a time invariant offset must be added to assess absolute transport (Kanzow et al., 2007). In contrast, the Surcouf3D product is an estimate of the absolute geostrophic velocities at any level from the surface to 1500 m, so the total transport at 25°N in the 1500 first meters can be theoretically derived from the summation of its three components (the geostrophic component evaluated from Surcouf3D and the Ekman and Florida current components) without adding any offset. However, errors inherent in the Surcouf3D fields, once integrated over the section, can break the mass balance. For instance, the transport is very sensitive to an error in the east–west MDT gradient. The limited vertical extension of the Surcouf3D field also prevents us from imposing mass conservation over the water column through an offset computation. Despite this difficulty, there is good agreement with other AMOC estimates (shown in the following) which gives us confidence in the robustness of the Surcouf3D fields.

A quantity commonly used to study overturning is its maximum value at depth that is reached at around 1000 m at 25°N (BR05; Hirschi et al., 2003). In the following we thus study the transport integrated from the surface to 1000 m. We first compute the meridional geostrophic transport integrated from the surface to 1000 m and from the Bahamas to Africa (upper mid-ocean geostrophic transport) using the Surcouf3D velocity field (blue circles in Fig. 8). The upper mid-ocean geostrophic transport was found to be significantly dependant on the chosen latitude, mainly due to the differences in circulation in the western part of the section as BR05 already pointed out. For instance the upper mid-ocean geostrophic transport in 2004 is −17.1 Sv at 24.5°N while it is −21.3 Sv if computed though the exact BR05 section (section at 24.5°N angled northwestward at 73°W to finish along 26.5°N to the Bahamas) including 2 Sv from the flow through the northwest Providence channel (BR05; Leaman et al., 1995). In Fig. 8, the different components of the maximum AMOC strength have therefore been computed along the exact BR05 section to allow for a rigorous comparison.

The Florida current transport (red stars in Fig. 8) is obtained from the cable measurements that have been performed daily from 1982 (Larsen, 1992). The meridional Ekman transport (green squares in Fig. 8) is computed using the 80 km resolution wind stress maps from the ERA INTERIM reanalysis (Simmons et al., 2007). Finally the maximum AMOC strength time series (black triangles in Fig. 8) is inferred by adding the three previous components for each month from 1993 to 2008.

The upper mid-ocean geostrophic transport and thus the AMOC strength time series are characterized by a strong

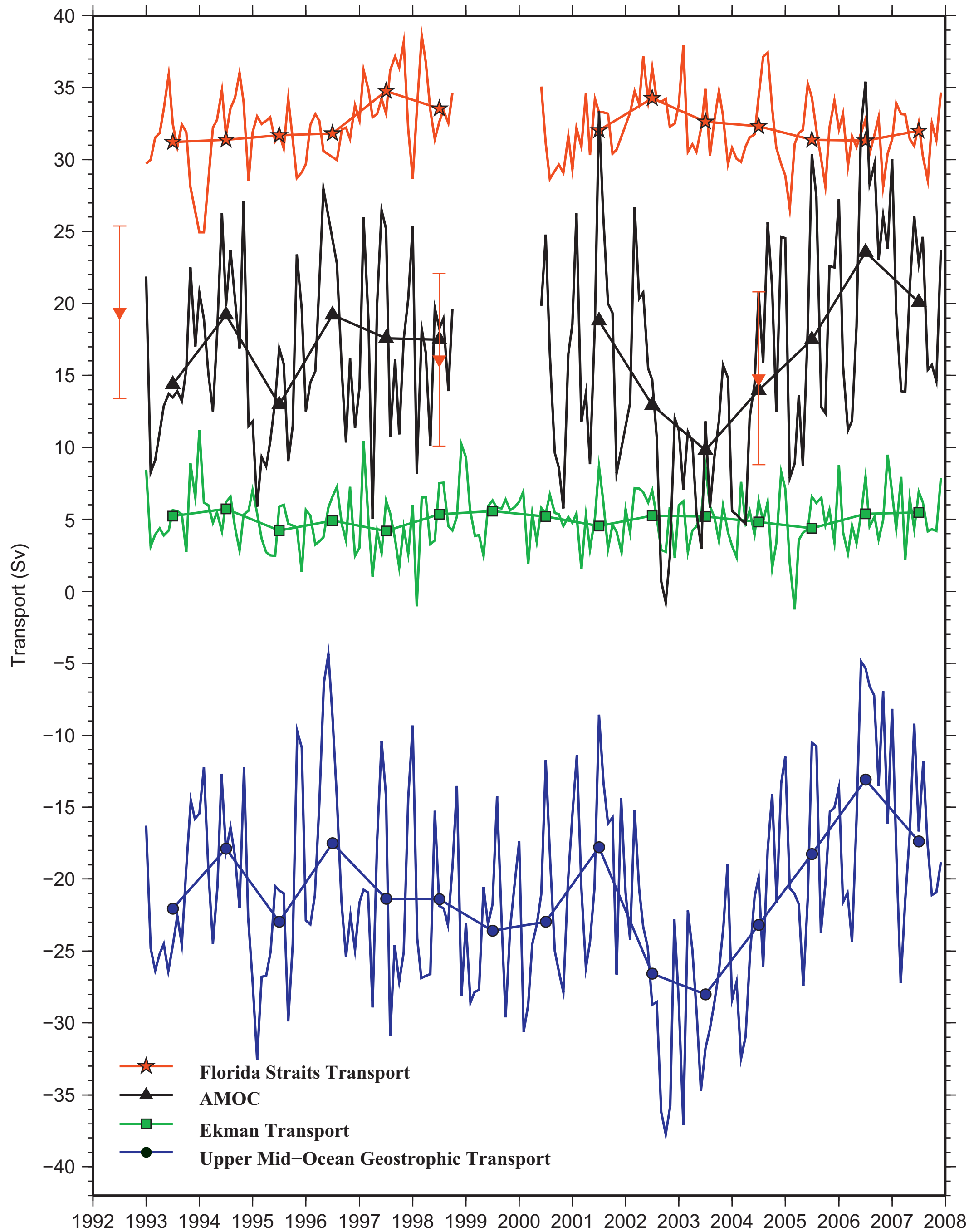


**Fig. 8.** Monthly (thin lines) and yearly (thick lines) time series of the Florida Strait Transport (red stars), Ekman Transport (green squares), upper mid-ocean geostrophic Transport computed from Surcouf3D (blue circles) and AMOC maximum strength (black triangles) through the BR05 section at 25°N for the 1993–2008 period. Red inverted triangles represent results from BR05 with the associated error bars. The gap from November 1998 to May 2000 is due to a gap in the Florida transport estimate. (For interpretation of the references to color in this figure legend, the reader is referred to the web version of this article.)

variability at both seasonal to interannual time scales. The AMOC strength has a mean value of 16 Sv with a full period yearly standard deviation of 2.4 Sv, while the monthly standard deviation is 7.1 Sv. In spite of this high variability, our method gives values close to the BR05 ones and within the BR05 error interval (red inverted triangles and error bars on Fig. 8): we find an annual mean AMOC intensity of 17.49 Sv compared to 16.1 Sv in 1998 and of 13.96 Sv compared to 14.8 Sv in 2004 (black triangles and red inverted triangles in Fig. 8). However, while BR05 suggested a slow down of 30%, the complete time series computed with Surcouf3D does not show any clear trend and is dominated by a high seasonal to interannual variability.

We then have compared our results to the values obtained from the GLORYS reanalysis and the RAPID-MOCHA array over April 2004 to September 2007 (Fig. 9). To be consistent with the AMOC time series estimated from the RAPID-MOCHA array, we have computed the maximum AMOC strength across the same section which starts at about 26.5°N at the western boundary and ends at about 27.5°N at the eastern boundary. Good agreement is obtained for seasonal cycles (thick lines in Fig. 9) computed with the three different datasets with a minimum in spring and a maximum in autumn. In 2004 the maximum in the Surcouf3D time series occurs slightly later than in the other time series. This is due to an overestimation of the Surcouf3D transport in

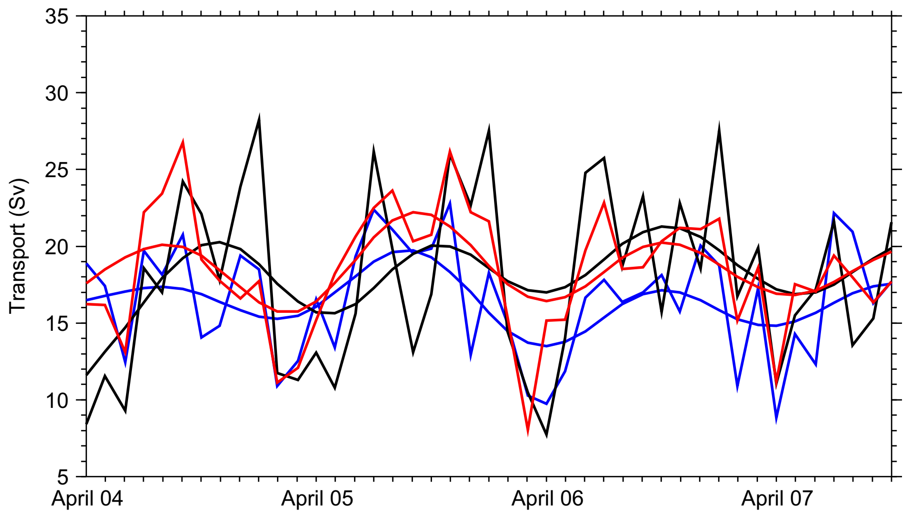


**Fig. 9.** Monthly (thin lines) and 12-month-filtered (thick lines) time series of the maximum strength of the AMOC at 26.5°N estimated using three different methods. In black: Surcouf3D, in blue: GLORYS and in red: RAPID-MOCHA array.

December 2004 and January 2005 which impacts on the 12-month filtered time series. Indeed, the maximum AMOC strength obtained from Surcouf3D shows a higher monthly variability (thin line) than the observations and the model reanalysis. Surcouf3D time series has a standard deviation of 5.59 Sv around a mean value of 19.27 Sv while RAPID-MOCHA (resp. GLORYS) time series has a standard deviation of 3.95 Sv (resp. 3.61 Sv) around a mean value of 18.48 Sv (17.44 Sv). The obtained overestimated variability is likely due to the overestimated mesoscale activity at depth mentioned in Section 3. However, the Surcouf3D time series resolves the extrema quite well (such as the maxima in September 2004 and November 2005 and the minima in February 2005 and April 2007) and is well correlated with the RAPID-MOCHA time series (correlation coefficient of 0.67 at the 99% significance level). A higher correlation coefficient (0.77) is obtained with GLORYS.

To quantify the error of our method for the AMOC computation at 26.5°N, we have used the GLORYS reconstructed geostrophic currents computed in Section 4.1 to compute the upper mid-ocean geostrophic transport. The reconstructed AMOC was then obtained by adding the Florida and Ekman transports, and was compared to the native GLORYS AMOC. The reconstructed field leads to an underestimated of the monthly averaged AMOC values of $1.6 \pm 0.4$ Sv over the April 2004 to September 2007 period where 0.9 Sv is due to the difference between the Florida current transport estimated from the cable measurements and from GLORYS. The simple thermal wind approximation is leading to a minor underestimate of the AMOC, possibly because of other physical processes present in the full GLORYS field.

## 6. Discussion and conclusions

A new observation-based estimate of the global 3D geostrophic circulation from the surface to 1500 m has been computed by merging altimetric data and a synthetic 3D thermohaline field through the thermal wind equation setting the reference level at the surface. The validity of the thermal wind equation was tested and it was found that the error of the method is less than 10% in most places outside the boundary layers and up to 20% in coastal areas away from the Ekman layer. In spite of the simplicity of the method, comparisons in the Atlantic Ocean to a model reanalysis from the Mercator Ocean system as well as to Argo floats and current meters velocities give very consistent results. This current field was used to compute a 1993–2008 long time series of the maximum AMOC strength at 25°N. Results are in good agreement with other studies (GLORYS, RAPID-MOCHA, Bryden et al., 2005). The AMOC strength time series is characterized by a very high seasonal and interannual variability and appears to have no statistically significant trend over the entire period.

Despite these promising results, we found that Surcouf3D is too energetic and overestimates the vertical penetration of the mesoscale activity which is well resolved at the surface from altimetry. This is most likely due to the synthetic thermohaline field which does not have enough vertical density gradient structure. This missing vertical structure would act to compensate for the surface altimetric signal which is added at each level to compute the absolute geostrophic currents following Eq. 2. For instance, the synthetic thermohaline field fails to resolve the strong density gradient associated with the Western Boundary Current off the Bahamas. This permanent structure is not resolved by the ARIVO climatology, the first guess of the synthetic field. This prevents us from reconstructing the local current shear at this specific location. Resolving the narrow boundary current system with its strong vertical and horizontal shear is very specific to this area and is pushing the limits of what we can resolve with a global 3D current product. However, we expect significant improvement from the use of a new thermohaline field (Guinehut et al., 2004, 2012; Larnicol et al., 2006) that combines the synthetic estimate based on historical statistics with instantaneous in-situ *T*/*S* profiles through an objective analysis scheme, thus improving the 3D density estimate. Preliminary results are quite encouraging, highlighting the importance of a sustained global in-situ array of *T*/*S* profile measurements in combination with satellite altimetry for the monitoring of the ocean state. A second limitation of the Surcouf3D field is the lack of information deeper than 1500 m but we are working on ways to extend the 3D oceanic circulation field down to the bottom using a *T*/*S* climatology or a projection onto baroclinic modes.

We also plan to extend the validation over the global ocean in order to test the accuracy of the Surcouf3D fields at different locations and to study the meridional overturning circulation at different key sections of the conveyor belt (Ganachaud, 2003). Monitoring the MOC is a delicate issue, firstly because of its high variability, as illustrated at 25°N, and secondly because it involves complex processes that are barely resolved by numerical models (Biastoch et al., 2008; Hirschi et al., 2003). In addition, currents flowing very close to the coast are not always well resolved by observations. As a consequence, cross validation of the MOC strength is essential (von Schuckmann et al., 2010). We are confident that the comparison of this new 3D current field with other existing studies based on observations, or numerical models, will help better understand and monitor this key quantity of the climate system.

## Acknowledgments

The authors would like to express their thanks to Michel Ollitrault and Jean-Philippe Rannou for providing their ANDRO atlas. They also would like to thanks the RAPID-MOCHA team for providing data from the array. Data from the RAPID-WATCH MOC monitoring project are funded by the Natural Environment Research Council and are freely available from www.noc.soton.ac.uk/rapidmoc. The realization of GLORYS1 global ocean reanalysis had the benefit of the Grants that Groupe Mission Mercator Coriolis, Mercator-Ocean, and CNRS/INSU attributed to the GLORYS project, and the support of the European Union FP7 via the MYOCEAN project. The altimeter products were produced by Ssalto/Duacs and distributed by Aviso with support from CNES. The Florida Current cable and section data are made freely available on the Atlantic Oceanographic and Meteorological Laboratory web page (www.aoml.noaa.gov/phod/floridacurrent/) and are funded by the NOAA Office of Climate Observations. Helpful comments from E. Greiner, N. Ferry and the reviewers were appreciated.

## References

Biastoch, A., Böning, C.W., Getzlaff, J., Molines, J., Madec, G., 2008. Causes of interannual–decadal variability in the meridional overturning circulation of the midlatitude North Atlantic Ocean. J. Climate 21, 6599–6615.

Bryden, H.L., Longworth, H.R., Cunningham, S.A., 2005. Slowing of the Atlantic meridional overturning circulation at 25°N. Nature 438 (7068), 655–657, http://dx.doi.org/10.1038/nature04385.

Cabanes, C., Lee, T., Fu, L.-L., 2008. Mechanisms of interannual variations of the meridional overturning circulation of the North Atlantic Ocean. J. Phys. Oceanogr. 38 (2), http://dx.doi.org/10.1175/2007JPO3726.1.

Carton, J.A., Chepurin, G., Cao, X., Giese, B.S., 2000a. A Simple Ocean Data Assimilation analysis of the global upper ocean 1950–1995, Part 1: methodology. J. Phys. Oceanogr. 30, 294–309.

Carton, J.A., Chepurin, G., Cao, X., 2000b. A Simple Ocean Data Assimilation analysis of the global upper ocean 1950–1995 Part 2: results. J. Phys. Oceanogr. 30, 311–326.

Cunningham, S.A., Kanzow, T., Rayner, D., Baringer, M.O., Johns, W.E., Marotzke, J., Longworth, R., Grant, E.M., Hirschi, J.J.-M., Beal, L.M., Meinen, C.S., Bryden, H.L., 2007. Temporal variability of the Atlantic meridional overturning circulation at 26.5°N. Science 317 (5840), 935–938, http://dx.doi.org/10.1126/science.1141304.

Dhomps, A.-L., Guinehut, S., Le Traon, P.-Y., Larnicol, G., 2011. A global comparison of Argo and satellite altimetry observations. Ocean Sci. 7, 175–183.

Emery, W.J., Thomson, R.E., 1998. Data Analysis Methods in Physical Oceanography. Pergamon (634 pp.).

Ferry, N., Parent, L., Garric, G., Barnier, B., Jourdain, N.C., the Mercator Ocean team, 2010. Mercator Global Eddy Permitting Ocean Reanalysis GLORYS1V1: Description and Results. Mercator Ocean Quarterly Newsletter #36, January 2010, pp. 15–27.

Gaillard, F., Charraudeau, R., 2008. New Climatology and Statistics Over the Global Ocean. MERSEA-WP05-CNRS-STR-001-1A.

Ganachaud, A., 2003. Large-scale mass transports, water mass formation, and diffusivities estimated from World Ocean Circulation Experiment (WOCE) hydrographic data. J. Geophys. Res. 108 (C7), 3213, http://dx.doi.org/10.1029/2002JC001565.

Guinehut, S., Le Traon, P.Y., Larnicol, G., Philipps, S., 2004. Combining Argo and remote-sensing data to estimate the ocean three-dimensional temperature fields—a first approach based on simulated observations. J. Mar. Syst. 46 (1–4), 85–98, http://dx.doi.org/10.1016/j.jmarsys.2003.11.022.

Guinehut, S., Le Traon, P., Larnicol, G., 2006. What can we learn from global altimetry/hydrography comparisons? Geophys. Res. Lett, 33, http://dx.doi.org/10.1029/2005GL025551.

Guinehut, S., Dhomps, A.-L., Larnicol, G., LeTraon, P.-Y., 2012. High resolution 3-D temperature and salinity fields derived from in situ and satellite observations. Ocean Sci. Discuss. 9, 1313–1347, http://dx.doi.org/10.5194/osd-9-1313-2012.

Hirschi, J., Baehr, J., Marotzke, J., Stark, J., Cunningham, S.A., Beismann, J., 2003. A monitoring design for the Atlantic meridional overturning circulation. Geophys. Res. Lett. 30 (7), 1413, http://dx.doi.org/10.1029/2002GL016776.

Johns, W.E., Beal, L.M., Baringer, M.O., Molina, J.R., Cunningham, S.A., Kanzow, T., Rayner, D., 2008. Variability of shallow and deep Western Boundary Currents off the Bahamas during 2004–05: results from the 26°N RAPID–MOC array. J. Phys. Oceanogr. 38, 605–623, http://dx.doi.org/10.1175/2007JPO3791.1.

Johns, W.E., Kanzow, T., Zantopp, R., 2005. Estimating ocean transports with dynamic height moorings: an application in the Atlantic Deep Western Boundary Current at 26°N. Deep-Sea Res. I 52 (8), 1542–1567, http://dx.doi.org/10.1016/j.dsr.2005.02.002.

Kanzow, T., Send, U., Zenk, W., Chave, A., Rhein, M., 2006. Monitoring the integrated deep meridional flow in the tropical North Atlantic: long-term performance of a geostrophic array. Deep-Sea Res. I 53 (3), 528–546, http://dx.doi.org/10.1016/j.dsr.2005.12.007.

Kanzow, T., Cunningham, S.A., Rayner, D., Hirschi, J.J., Johns, W.E., Baringer, M.O., Bryden, H.L., Beal, L.M., Meinen, C.S., Marotzke, J., 2007. Observed flow compensation associated with the MOC at 26.5°N in the Atlantic. Science 317 (5840), 938–941, http://dx.doi.org/10.1126/science.1141293.

Larnicol, G., Guinehut, S., Rio, M.H., Drevillon, M., Faugere, Y., Nicolas, G., 2006. The Global observed ocean products of the French Mercator project. In: Proceedings of the Symposium on 15 Years of Progress in Radar Altimetry 13–18 March 2006, Venice, Italy.

Larsen, J.C., 1992. Transport and heat flux of the Florida Current at 27°N derived from cross-stream voltages and profiling data: theory and observations. Philos. Trans. R. Soc. London A 338, 169–236.

Le Vine, D.M., Lagerloef, G.S.E., Colomb, F.R., Yueh, S.H., Pellerano, F.A., 2007. Aquarius: an instrument to monitor sea surface salinity from space. IEEE Trans. Geosci. Remote Sensing.

Leaman, K.D., Vertes, P.S., Atkinson, L.P., Lee, T.N., Hamilton, P., Waddell, E., 1995. Transport, potential vorticity, and current/temperature structure across Northwest Providence and Santaren Channels and the Florida Current off Cay Sal Bank. J. Geophys. Res. 100 (C5), 8561–8569.

Lique, C., Garric, G., Treguier, A., Barnier, B., Ferry, N., Testut, C., Girard-Ardhuin, F., 2011. Evolution of the Arctic Ocean salinity, 2007–08: contrast between the Canadian and the Eurasian Basins. J. Climate 24 (6), 1705–1717, http://dx.doi.org/10.1175/2010JCLI3762.1.

Meijers, A.J.S., Bindoff, N.L., Rintoul, S.R., 2011. Estimating the four-dimensional structure of the Southern Ocean using satellite altimetry. J. Atmos. Oceanic Technol.

Ollitrault, M., Lankhorst, M., Fratantoni, D., Richardson, P., Zenk, W., 2006. Zonal intermediate currents in the equatorial Atlantic Ocean. Geophys. Res. Lett. 33, L05605, http://dx.doi.org/10.1029/2005GL025368.

Ollitrault, M., Rannou, J.P., 2010. ANDRO: An Argo-based Deep Displacement Atlas. Mercator Ocean Quarterly Newsletter #37, April 2010, pp. 27–34.

Reynolds, R.W., Smith, T.M., Liu, C., Chelton, D.B., Casey, K.S., Schlax, M.G., 2007. Daily high-resolution-blended analyses for sea surface temperature. J. Climate 20, 5473–5496, http://dx.doi.org/10.1175/2007JCLI1824.1.

Rio, M.-H., Schaeffer, P., 2005. The estimation of the ocean mean dynamic topography through the combination of altimetric data, in-situ measurement and GRACE geoid. In: Proceedings of the GOCINA International Workshop, Luxembourg.

von Schuckmann, K., Drévillon, M., Ferry, N., Mulet, S., Rio, M.-H., 2010. Global Ocean Indicators. Mercator Ocean Quarterly Newsletter #37, April 2010, pp. 20–28.

Silvestrin, P., Berger, M., Kerr, Y., Fontin, J., 2001. ESA's second earth explorer opportunity mission: the soil moisture and ocean salinity mission-SMOS. IEEE Geosci. Remote Sensing Newsl.

Simmons, A., Uppala, S., Dee, D., Kobayashi, S., 2007. ERA-Interim: new ECMWF reanalysis products from 1989 onwards. ECMWF Newsl. 110, 25–35.

SSALTO/DUACS, 2011. User Handbook: MSLA and MADT Near-Real Time and Delayed Products. C.L.S., Ramonville St. Agne, France.

Taylor, K.E., 2001. Summarizing multiple aspects of model performance in a single diagram. J. Geophys. Res. 106 (D7), 7183–7192.

Willis, J.K., Roemmich, D., Cornuelle, B., 2003. Combining altimetric height with broadscale profile data to estimate steric height, heat storage, subsurface temperature, and sea-surface temperature variability. J. Geophys. Res. 108 (C9), 3292, http://dx.doi.org/10.1029/2002JC001755.

Willis, J.K., Fu, L.-L., 2008. Combining altimeter and subsurface float data to estimate the time-averaged circulation in the upper ocean. J. Geophys. Res. 113, C12017, http://dx.doi.org/10.1029/2007JC004690.

Willis, J.K., 2010. Can in situ floats and satellite altimeters detect long term changes in Atlantic Ocean overturning? Geophys. Res. Lett. 37, L06602, http://dx.doi.org/10.1029/2010GL042372.

Wunsch, C., 1996. The Ocean Circulation Inverse Problem. Cambridge University Press.

Zheng, Y., Giese, B.S., 2009. Ocean heat transport in Simple Ocean Data Assimilation: STructure and mechanisms. J. Geophys. Res. 114, C11009, http://dx.doi.org/10.1029/2008JC005190.